Honors Undergraduate Theses

UCF Theses and Dissertations

2016

Atmospheric, Orbital, and Eclipse-Depth Analysis of the Hot Jupiter HAT-P-30-WASP-51Ab

Andrew SD Foster
University of Central Florida

Showcase of Text, Archives, Research & Scholarship

ATMOSPHERIC, ORBITAL, AND ECLIPSE-DEPTH ANALYSIS OF THE HOT JUPITER HAT-P-30-WASP-51Ab

by

ANDREW SD FOSTER

A thesis submitted in partial fulfillment of the requirements
for the Honors in the Major Program in Physics
in the College of Sciences
and in the Burnett Honors College
at the University of Central Florida
Orlando, Florida

Spring Term, 2016

Thesis Chair: Joseph Harrington, PhD

ABSTRACT

HAT-P-30-WASP-51b is a hot-Jupiter exoplanet that orbits an F star every 2.8106 days at a distance of 0.0419 AU. Using the Spitzer Space Telescope in 2012 (Spitzer Program Number 70084) we observed two secondary eclipses at 3.6 and 4.5 μm. We present eclipse-depth measurements of 0.177 ± 0.018 % and 0.247 ± 0.024 % and estimate the infrared brightness temperatures to be 1990 ± 110 K and 2080 ± 130 K for these two channels, respectively, from an analysis using our Photometry for Orbits, Eclipses, and Transits (POET) pipeline. These may be grazing eclipses. We also refine its orbit using our own secondary-eclipse measurements in combination with radial-velocity and transit observations from both professional and amateur observers. Using only the phase of our secondary eclipses, we can constrain $e\cos(\omega)$ where e is the orbital eccentricity and ω is the argument of periastron to 0.0058 ± 0.00094. This is the component of eccentricity in the plane of view,. This small but non-zero eccentricity is independent of the effects that stellar tides have on radial-velocity data. When including radial velocity data in our model, our Markov chain finds an $e\cos(\omega)$ of 0.0043 ± 0.0007. We constrain the atmospheric temperature profile using our Bayesian Atmospheric Radiative Transfer code (BART), a large lower bound (700 km) for the scale height, and the potential for high quality transit spectroscopy observations.

TABLE OF CONTENTS

LIST OF FIGURES

LIST OF TABLES

CHAPTER 1: INTRODUCTION

Thanks to the Kepler Space Telescope, humanity now knows of almost two thousand planets that orbit other stars (The Extrasolar Planet Encyclopedia: exoplanet.eu). These exoplanets and their properties can reveal important information about the formation of solar systems and the Earth. Studying these planets helps to answer some of humanity's oldest questions: where did we come from and how did we get here?

To answer these important questions, we must first closely study many exoplanet systems and look for trends in the data. Although we can neither see nor observe most of these planets directly, we can glean much information by indirect means. By measuring the Doppler shift of the planets' host stars over the course of an orbit, we can determine the mass of the planets and the shape of their orbits (Johnson et al. 2011). Some planets pass in between their stars and the Earth, blocking out the light from their stars and giving us a measurement of the planets' radii (Johnson et al. 2011). These events are called transits and these planets are called transiting exoplanets. Often, transiting exoplanets also pass behind their stars causing a dip in infrared light corresponding the temperature of the planet (Stevenson et al. 2012). These events are called secondary eclipses. Because atmospheres have different opacities at different wavelengths, by taking measurements across the spectrum probes different levels of the atmospheres. From this we can construct an atmospheric model for these planets (Stevenson et al. 2012). Furthermore, the timing of these transits and eclipses can help us constrain the orbits of the planets (Stevenson et al. 2012). Currently, we are only able to do this for the largest and hottest exoplanets, hot Jupiters and hot Neptunes, with any significant precision. However, the techniques that we are using for these gas giants can be used on rockier, terrestrial planets once the next generation of telescopes are operational.

Purpose

By studying exoplanets and their atmospheres we can learn more about how planets form. In particular, hot Jupiters are interesting because the extreme conditions in their atmospheres can give us a better understanding of how atmospheres in general work. These atmospheric retrieval techniques and photometric techniques have pushed the boundaries of what is possible to do with a telescope and will continue to do so going forward.

In my thesis, I will analyze of the orbit and atmosphere of the hot-Jupiter HAT-P-30-WASP-51Ab using secondary eclipse observations taken by the *Spitzer* Space Telescope in 2012 (Program 70084) as well as data from literature and amateur sources.

CHAPTER 2: LITERATURE REVIEW

To begin, I will explain the components of HAT-P-30-WASP-51Ab's name. It was discovered independently by the Hungarian Array of Telescopes Network (HATNet) and the Wide Angle Search for Planets (WASP). The HATNet team published their findings on the planet first, which is why their name is first (Johnson et al. 2011). It was the thirtieth planet that they found, hence the HAT-P-30 part of the name, with the "P" standing for planet. It was the fifty-first planet found by the WASP team, hence the WASP-51 part of the name (Enoch et al. 2011). This star system is a binary system of an F type star and an M dwarf separated by about 750 AU (Ngo etal 2015). The "A" in the name indicates that the planet orbits only the primary star (the F-type), while the "b" at the end indicates that this is the first planet found in this system.

The drop in flux during the secondary eclipse of an exoplanet is a direct measurement of the light emitted from the planet. As such, observing secondary eclipses at various wavelengths is a useful tool for analyzing the atmospheres of these planets. Eclipse depths have been commonly used in this manner ever since their first detection of secondary eclipse events by Charbonneau et al. (2005) and Deming et al. (2005). Since the planet-to-star flux ratios typically lie below $\times 10^{-3}$ while *Spitzer* systematics are on the order of $\times 10^{-2}$, we must use a variety of statistical methods to peer through the noise. Fortunately, *Spitzer* systematic errors have undergone extensive research and modeling (Seager & Deming 2010, Stevenson et al. 2012a, Deming et al. 2015).

The Infrared Array Camera (IRAC) is able to observe at various wavelengths that penetrate a planet's atmosphere to various altitudes. After isolating the secondary-eclipse light curve, we fit an atmospheric model to the eclipse depths in these bands using our Bayesian Atmospheric Radia-

tive Transfer (BART) code (Cubillos 2016, Blecic 2016).

Secondary eclipse observations can also help to constrain the orbit of a planet. The Arras et al. (2012) effect of stellar tides can exaggerate measures of eccentricity from radial velocity curves, but a nonzero value for the component of eccentricity perpendicular to the line of sight, $e\cos(\omega)$ where e is the eccentricity and ω is the argument of periapsis, from eclipse timing can provide a detection of eccentricity that is independent of stellar tides because it relies only on the geometry of the orbit and Kepler's second law.

HAT-P-30-WASP-51Ab (Johnson et al. 2011) is a low density hot Jupiter, about half as dense as Saturn at 0.37 ± 0.05 g cm^{-3} with a radius of 1.340 ± 0.065 R_{Jup} and a mass of 0.711 ± 0.028 M_{Jup}, where R_{Jup} and M_{Jup} are the radius and mass, respectively, of Jupiter. It is in an oblique ($\beta = 73.5° \pm 9.0°$) orbit around a hot F-type star (HAT-P-30-WASP-51A), which is 6304 ± 88 K, with radius 1.21 ± 0.05 $R_{\odot}$, mass 1.24 ± 0.04 $M_{\odot}$, and metallicity [Fe/H] $= -0.13 \pm 0.08$. $R_{\odot}$ and $M_{\odot}$ are the radius and mass, respectively, of the Sun. There is a companion star in the system, an M dwarf with temperature 3634 ± 29 K at 750 AU from the primary star (Ngo et al. 2015). The planet was discovered in 2011 by both the Hungarian Automated Telescope Network (HATNet) (Johnson et al. 2011) and the Wide Angle Search for Planets (WASP) projects via transit observations (Enoch et al. 2011).

This paper analyzes our two eclipses of HAT-P-30-WASP-51Ab with all available transit and radial velocity data. Section 3 details our observations. Section 3 describes the data analysis. Section 3 presents our analysis of the planet's orbit. Section 3 gives our atmospheric model.

CHAPTER 3: METHODOLOGY and FINDINGS

Observations

We analyzed two secondary-eclipse light curves of HAT-P-30-WASP-51Ab from the *Spitzer Space Telescope*'s Infrared Array Camera (IRAC) at 3.6 and 4.5 μm, *Spitzer* Program number 70084, PI Joseph Harrington. Both observations were conducted in subarray mode and consisted of 12416 frames. The 3.6 μm observation was conducted on January 3, 2012 between the times of 09:16:19.589 and 16:12:33.552, and the 4.5 μm observation was conducted on January 17, 2012 between the times of 10:42:13.975 and 17:38:28.038.

Photometry

We analyzed the data using the Photometry for Orbits, Eclipses and Transits (POET) pipeline (Stevenson et al. 2010, Campo et al. 2011, Nymeyer et al. 2011, Stevenson et al. 2012a,b, Cubillos et al. 2013). We used Basic Calibrated Data (BCD) frames processed through the *Spitzer* pipeline S19.1.0.

To locate the centers of the two stars (see Figure 3.1), we fit two Gaussian centroids to the images. Then we fit a *Spitzer* TinyTim PSF to the companion star and subtracted its flux, following Cubillos et al. (2013).

We then performed aperture photometry on the images, with aperture sizes varying from 1.5 to

5 pixels at quarter-pixel increments. To each photometry dataset, we then fit the following light-curve model (full details in Stevenson et al. 2012a):

$$F(x,y,t) = F_s E(t) R(t) M(x,y) \qquad (3.1)$$

where $F(x,y,t)$ is the measured flux centered at position (x,y) on the detector at time t, F_s is the (constant) system flux outside of secondary eclipse, $E(t)$ is the eclipse light-curve model from Mandel & Agol (2002), $R(t)$ corrects for *Spitzer*'s time-dependent sensitivity ramp, and $M(x,y)$ is the position-dependent intrapixel sensitivity model.

To correct for *Spitzer*'s systematics, we fit each combination of three ramp models (none, linear, quadratic) and two interpolation schemes (nearest neighbor and BiLinearly Interpolated Subpixel Sampling, BLISS) using a differential-evolution Markov chain (DEMC).

Stevenson et al. (2012a) describes BLISS, a method for mapping intrapixel sensitivity differences. BLISS bins frames based on the center position of the star (from the Gaussian centroid fitting above), and weights each of those bins by the average flux of the frames inside. We used a minimum bin size of four frames. Nearest neighbor interpolation divides out the sensitivity weight of the nearest bin to the center of the star in that frame, while BLISS bilinearly interpolates between bins and divides out that interpolated subpixel sensitivity.

In both channels, the dataset with an aperture size of 2.5 pixels yeilded the best standard deviation of the normalized residuals (SDNR), so we use those photometry data for all further steps. In channel 1 a quadradic ramp model with BLISS mapping provided the best fit, while in channel 2 a linear ramp model with BLISS mapping provided the best fit.

We found that we were better able to constrain the parameters of these fits when performing a joint fit to both channels at once while equating the eclipse midpoint phases, durations, and ingress/egress times. All runs converged according to the Gelman-Rubin statistic.

The best-fit light curve models are in Figure 3.2, and the best-fit parameters with uncertainties are found in Table 3.1.

The duration of totality is within 1σ of zero, indicating a likely grazing eclipse. However, the eclipses must be close to full considering that the brightness temperature in both channels is larger than the theoretical equilibrium temperature of 1700 ± 20 K assuming zero albedo and uniform redustribution of stellar flux. Most, if not all, of the brightness from this planet gets eclipsed by its host star.

Orbit

We fit an orbit using the method described in Campo et al. (2011). We used radial velocity data from the two discovery papers as well as the publicly released followup radial velocity data from the HATNet team (Johnson et al. 2011, Enoch et al. 2011, Bakos et al. 2015). Transit midpoint timing data came from the discovery papers and from amateur observers who posted their findings to TRESCA's Exoplanet Transit Database (ETD), see Table 3.2. Eclipse midpoint times from the present work constrain the eccentricity and period.

We were able to improve all orbital parameters, enumerated in Table 3.3. The semimajor axis (a) was not fit by the Markov chain, but was calculated from the period of the planet's orbit using Kepler's third law and the mass of the star from Johnson et al. (2011). All other parameters in Table 3.3 were fit by the Markov chain. Note the non-zero eccentricity in $e\cos(\omega)$, the component of eccentricity in the plane of view. Stellar tides have been known to cause a false positive for eccentricity in radial velocity data (Arras et al. 2012). Using the following equation derived from the geometry of an ellipse and Kepler's second law:

$$e\cos(\omega) = \frac{\pi}{2}(\phi - 0.5),\tag{3.2}$$

where ϕ is the secondary-eclipse midpoint time, we can show that this planet has a small but non-zero eccentricity of 0.0058 ± 0.0009. This uses only the secondary-eclipse midpoint timings, which are independent of the effects of stellar tides.

Because this planet has either a grazing eclipse or very close to a grazing eclipse when viewed from Earth, we know that the impact parameter of the planet relative to its star must be approximately the radius of its star minus the radius of the planet when viewed from the Earth. In essence, we know that:

$$b \approx R_* - R_p = (1 + e\sin(\omega))a\cos(i).\tag{3.3}$$

Because we know a from the work above, and Johnson et al. (2011) provides R_* and i the latter from the analysis of the Rossiter-McLaughlin effect and R_* from Johnson et al. (2011) we might hope for a better constraint on $e\sin(\omega)$ by rearranging equation 3.3 to:

$$e\sin(\omega) = 1 - \frac{R_* - R_p}{a\cos(i)} = -0.076 \pm 0.085,\tag{3.4}$$

8

but the uncertainties are worse in this case than those from the Markov chain.

Although we do not get a significant result for $e\sin(\omega)$, we do for $e\cos(\omega)$. This is an effective lower bound on the eccentricity of the planet.

Because the planet has a significantly non-zero eccentricity, we investigate the planet's circularization timescale (τ_{circ}) with the Mardling (2007) equation,

$$\tau_{circ} = \frac{2}{21n_p}\left(\frac{Q_p}{k_p}\right)\left(\frac{m_p}{m_*}\right)\left(\frac{a_p}{R_p}\right)^5, \tag{3.5}$$

where n_p is the orbitial frequency, Q_p is the tidal quality factor (Goldreich & Soter 1966, Mardling 2007), and k_p is the tidal Love number of the planet. Due to this planet's low density, we adopt a Saturn-like Love number of $k_p = 0.3$. Thus the only unknown factor in this equation is Q_p. With $Q_p = 10^6$, typical for a gas giant (Wu 2005), $\tau_{circ} = 2 \times 10^9$ years, which is on the order of magnitude of the stellar age from Johnson et al. (2011). However, perturbations from the second star should increase the circularization timescale, so it is not unreasonable that the planet's orbit is still circularizing. This calculation also does not take into account the perturbative effects of the second star in this system, which will likely increase the circularization timescale. It is not unreasonable that the planet's orbit is still circularizing.

9

Atmosphere

To model this planet's atmosphere, we use the Bayesian Atmospheric Radiative Transfer (BART) code (Cubillos 2016, Blecic 2016). BART uses a radiative transfer model to generate a spectrum for a model planet with a given pressure-temperature profile and given molecular abundances. It then integrates that spectrum to find the planets brightness, and therefore eclipse depth, in a certain bandpass. It uses a Markov chain to vary the molecular abundances and pressure temperature profile in order to explore the parameter space and find a constraint on these parameters.

This code operates under the assumption that the eclipse depth is representative of all of the flux from the planet. If the planet has grazing eclipses, the flux from the planet will be greater than the data indicate, and the brightness temperatures measured in eclipse will be less than those in the real planet, however unless there are spectral changes across the face of the planet, relative compositional inferences should not be badle affected. Because of the high brightness temperature of this planet, we assume that most of the planet is eclipsed by its star, and that therefore these values are approximately correct and close enough to not significantly affect the results of the BART run.

We ran BART for 5×10^6 iterations, when the Gelman-Rubin statistic for each parameter had converged to within 1% of unity. With only two channels, BART was unable to constrain blahblahblah We were unable to get significant constraints on the molecular abundances in the atmosphere of HAT-P-30-WASP-51Ab, but we were able to constrain some of the parameters of the atmosphere's one dimensional temperature-pressure profile, using the model described in Line et al. (2013) . The Bayesian posteriors for each parameter are shown in Figure 3.4, and two dimensional marginalizations of the posterior distribution shown in Figure 3.5. The Markov Chain favored a roughly isothermal atmosphere at around 2000 K. The distribution of PT profiles from the Markov chain

are shown in Figure 3.6.

We are unable to make any other claims about the atmosphere because our two data points, even if valid, are unable to constrain our models any better. More data would allow us to more precisely constrain the atmosphere of this planet. This is not unexpected. Mathematically, a model with n free parameters needs n data points to be fully constrained. It is common to only be able to constrain a temperature profile for a planet with a small number of data points.

The low density and high temperature yeild a large scale height.

$$H = \frac{kT}{Mg} \approx 700 \text{ km,} \tag{3.6}$$

where k is the Boltzmann constant, T is the brightness temperature from the POET run, M is the mean molecular mass (assumed to be 3.686×10^{-27} kg, that of Jupiter), and g, the acceleration due to gravity, is calculated from the mass and radius in Johnson et al. (2011), $0.711 \, M_{\text{Jup}}$ and $1.340 R_{\text{Jup}}$ respectively. Note that because this is potentially a grazing eclipse, the temperature of the planet and therefore its scale height could be even larger. A large scale height means that the layers of the planet's atmosphere are more widely separated, which means that during a transit a larger fraction of the star's light passes through the outer layers of the planet's atmosphere. A large scale height yeilds high quality transit spectroscopy.

Further, although this planet has a potentially grazing eclipse, it does not have a grazing transit (Johnson et al. 2011). Transit spectroscopy data for this planet's atmosphere should not only have a high signal to noise, it will also avoid this potential complication.
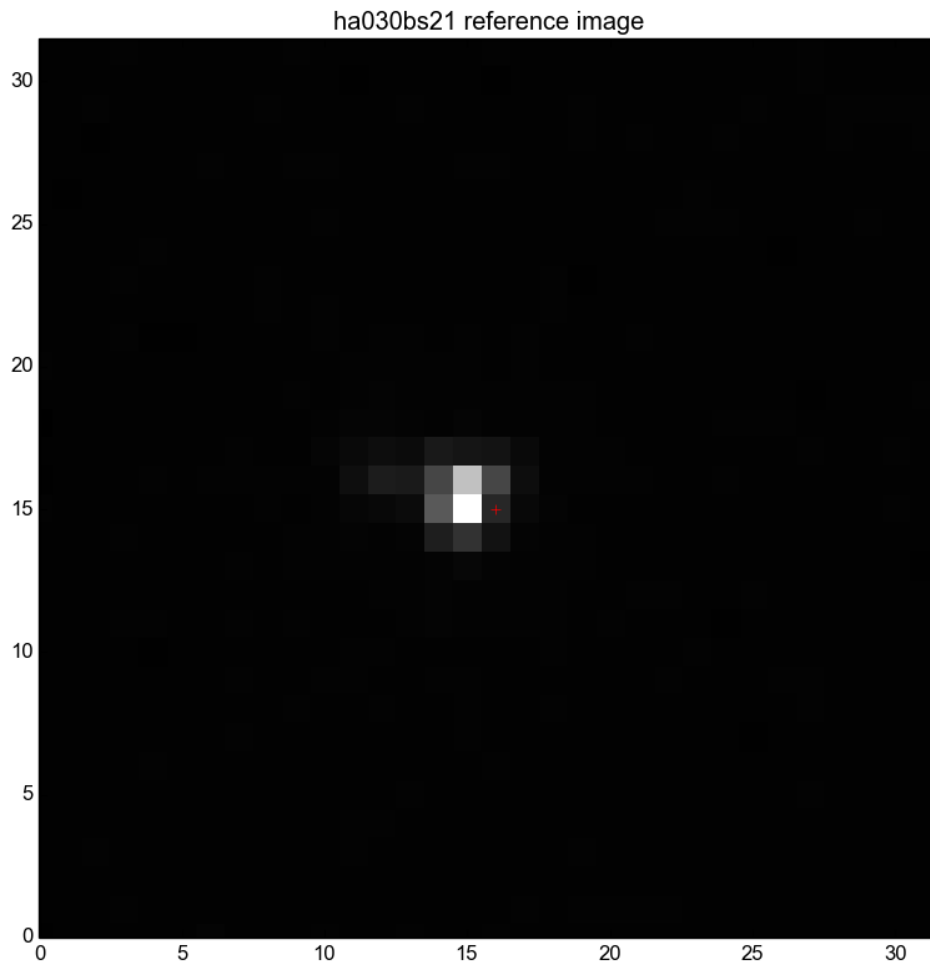
11

Figure 3.1:

Sample frame of system. The companion star is visible three pixels to the left and one pixel up from the center of the main star. The companion star has a Point Spread Function (PSF) that overlaps with the main star in the system.
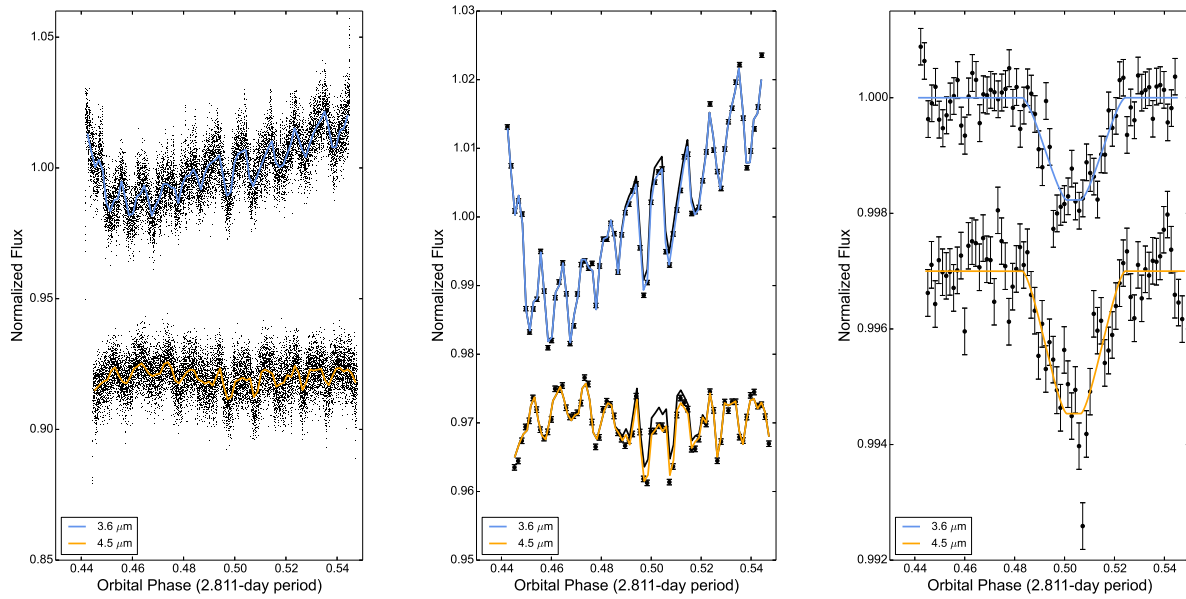
Figure 3.2:

Secondary-eclipse photometry for HAT-P-30-WASP-51Ab in *Spitzer* 3.6 μm and 4.5 μm bands, best-fit models in orange and blue, respectively. **Left:** Raw photometry with best-fit model of intrapixel and time ramp sensitivity. **Center:** Binned photometry with the best-fit models, orange for 3.6 μm and blue for 4.5 μm, and the best-fit models sans-eclipse in black for both channels. **Right:** Binned photometry of only the secondary eclipse (systematics divided out), with best-fit eclipse models. Error bars represent 1σ uncertainties.
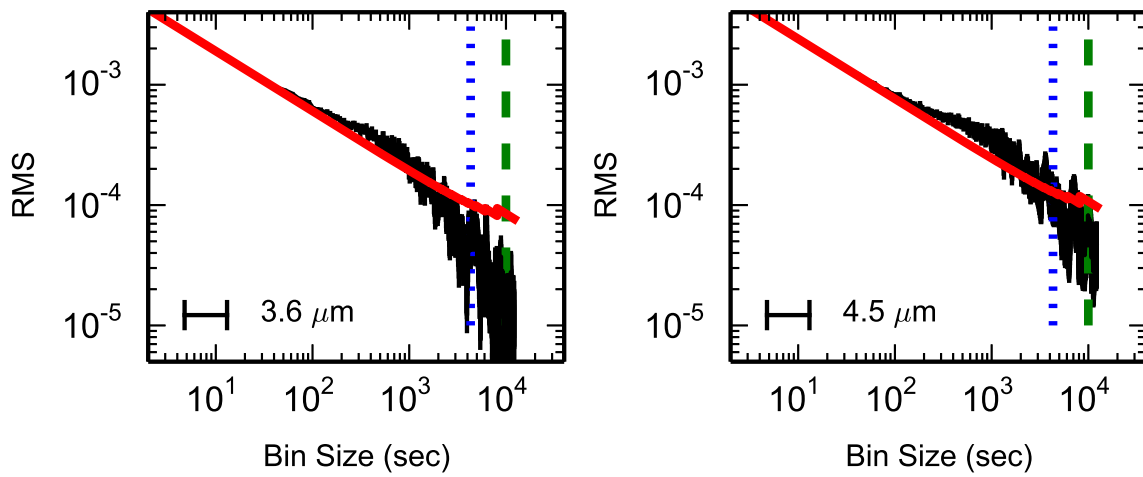
Figure 3.3:

The rms (root mean squared) of the fit residuals vs. bin size for 3.6 and 4.5 microns. The black curve is the residual with 1σ uncertainties. The red curve is the theoretical rms of Gaussian noise. The blue vertical line is at the timescale of ingress duration, and the green vertical line is at the timescale of eclipse duration. Fit residuals larger than the Gaussian noise would indicate red noise (but see Cubillos (2016)). Regardless, neither observation contains significant red noise on timescales between the ingress and eclipse duration.

Table 3.1: Best Fit Joint Eclipse Light Curve Parameters

Parameter	3.6 μm	4.5 μm
Array position ($\bar{x}$, pix)	14.92	14.96
Array position ($\bar{y}$, pix)	15.24	15.29
Position consistency	0.010	0.009
Position consistency	0.013	0.013
Aperture size (pix)	2.50	2.50
Sky annulus inner radius (pix)	7.0	7.0
Sky annulus outer radius (pix)	15.0	15.0
Eclipse depth (%)	0.177 $\pm$ 0.018	0.247 $\pm$ 0.024
Brightness Temperature (K)	1990 $\pm$ 110	2080 $\pm$ 130
Midpoint (orbits)	0.5037 $\pm$ 0.0006	joint
Transit midpoint (MJD_{UTC})	5930.0613$\pm$0.0017	5944.1143 $\pm$ 0.0017
Transit midpoint (MJD_{TDB})	5930.0620$\pm$0.0017	5944.1150 $\pm$ 0.0017
Eclipse duration (orbits)	0.041 $\pm$ 0.002	joint
Ingress/Egress time (orbits)	0.018 $\pm$ 0.003	joint
Eclipse Totality Time (orbits)	0.0056 $\pm$ 0.0064	joint
System flux: F_s (μ Jy)	56137 $\pm$ 6	36576 $\pm$ 3
Ramp: $R(t)$	Quadratic	Linear
Ramp, r_2	0.017 $\pm$ 0.003	-0.011 $\pm$ 0.004
Ramp, r_3	-0.23 $\pm$ 0.08	None
BLISS map ($M(x,y)$)	Yes	Yes
Min number of points per bin	4	4
Total frames	12416	12416
Frames used	12162	12200
Rejected frames (%)	2.05	1.74
Free parameters	7	3
AIC value	24372.0	24372.0
BIC value	24453.0	24453.0
SDNR	0.0042377	0.0053568
Uncertainty scaling factor	1.053	1.114
Photon-limited S/N (%)	79.32	82.62
Signal to Noise	9.61	10.44

Table 3.2: Amateur Observers

Transit Midpoint BJD(TDB)-2450000	Observer	Quality Rating
7089.42349±0.00111	Martin Zibar	3
7089.41389±0.00081	Marc Bretton	3
7061.31928±0.00195	Marc Bretton	3
7013.54120±0.00124	A Christophe, C Jacques, N Jean-Philippe	3
6982.62373±0.00107	Francesco Scaggiante, Danilo Zardin	3
6735.29291±0.00120	Shadic S., Rusov S.	3
6704.37213±0.00116	Marino G.	3
6687.50702±0.00170	Hentunen V. P.	3
6687.49936±0.00179	Sokov E. N., Gorshanov D.	3
6302.46166±0.00113	Gorshanov D, Sokov E, Vereshchagina I	3
6296.83773±0.00116	Shadic S.	3
6240.62493±0.00123	Naves R.	3
6001.72424±0.00141	Shadic S.	3
5976.42811±0.00118	Marino G.	3
5976.42751±0.00125	Gonzalez J.	3
5970.80607±0.00162	Shadic S.	3
5970.80491±0.00129	Shadic S.	3
5945.51283±0.00193	Gonzalez J.	3
5928.64834±0.00090	Naves R.	2
5914.59776±0.00134	Naves R.	3
5894.92544±0.00130	Shadic S.	3
5894.92165±0.00135	Shadic S.	3
5894.92008±0.00126	Shadic S.	3
5650.40068±0.00143	Uhlar R.	3
5644.77167±0.00208	Shadic S.	3
5571.70059±0.00020	B.Enoch et al. 2011	1
5456.46563±0.00037	J. A. Johnson et al., 2011	1

The Transiting ExoplanetS and Candidates group (TRESCA), (http://var2.astro.cz/EN/tresca/index.php) supply their data to the Exoplanet Transit Database (ETD), (http://var2.astro.cz/ETD/) which performs the uniform transit analysis described by Poddanã et al. (2010). The ETD web site provided the numbers in this table, which were converted from HJD (UTC) to BJD (TDB).

Table 3.3: Orbital Parameters

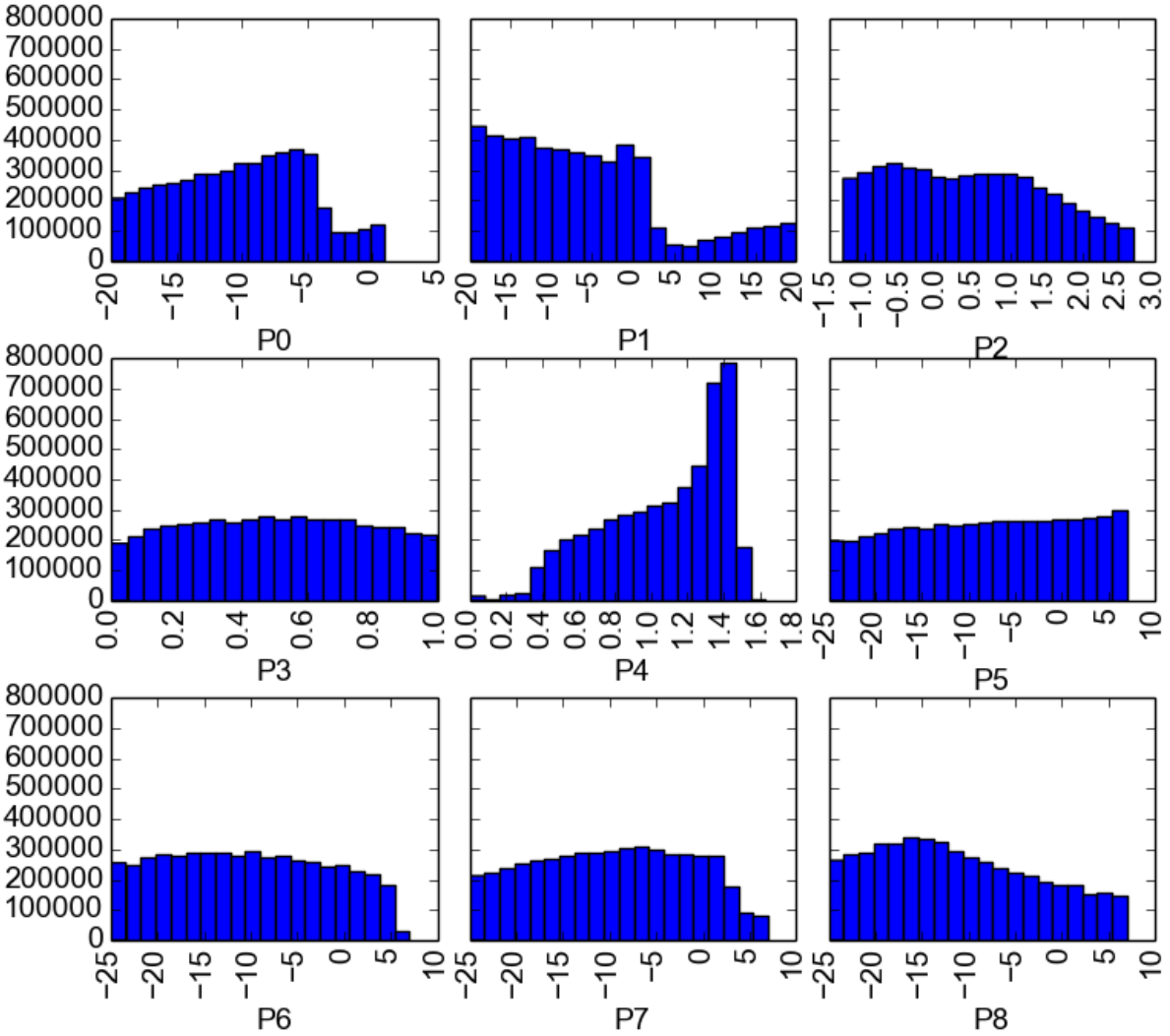| Parameter	Value	Error
$e\sin\omega$	-0.032	0.027
$e\cos\omega$	0.0043	0.0007
P (days)	2.810594	0.000002
a (AU)	0.04188	0.00046
t_0 (BJD_{TDB})	2455456.4682	0.0006
K (m/s)	91	3

Figure 3.4:

These are the posterior distributions of each parameter fed into the Markov chain. P0 through P8 represent the five parameters from the Line et al. (2013) PT profile function, and then the logarithms of the four molecular mixing ratios. In order: $\log(\kappa)$, $\log(g_1)$, $\log(g_2)$, α, β, $\log(M_{H_2O})$, $\log(M_{CO_2})$, $\log(M_{CO})$, and $\log(M_{CH_4})$.
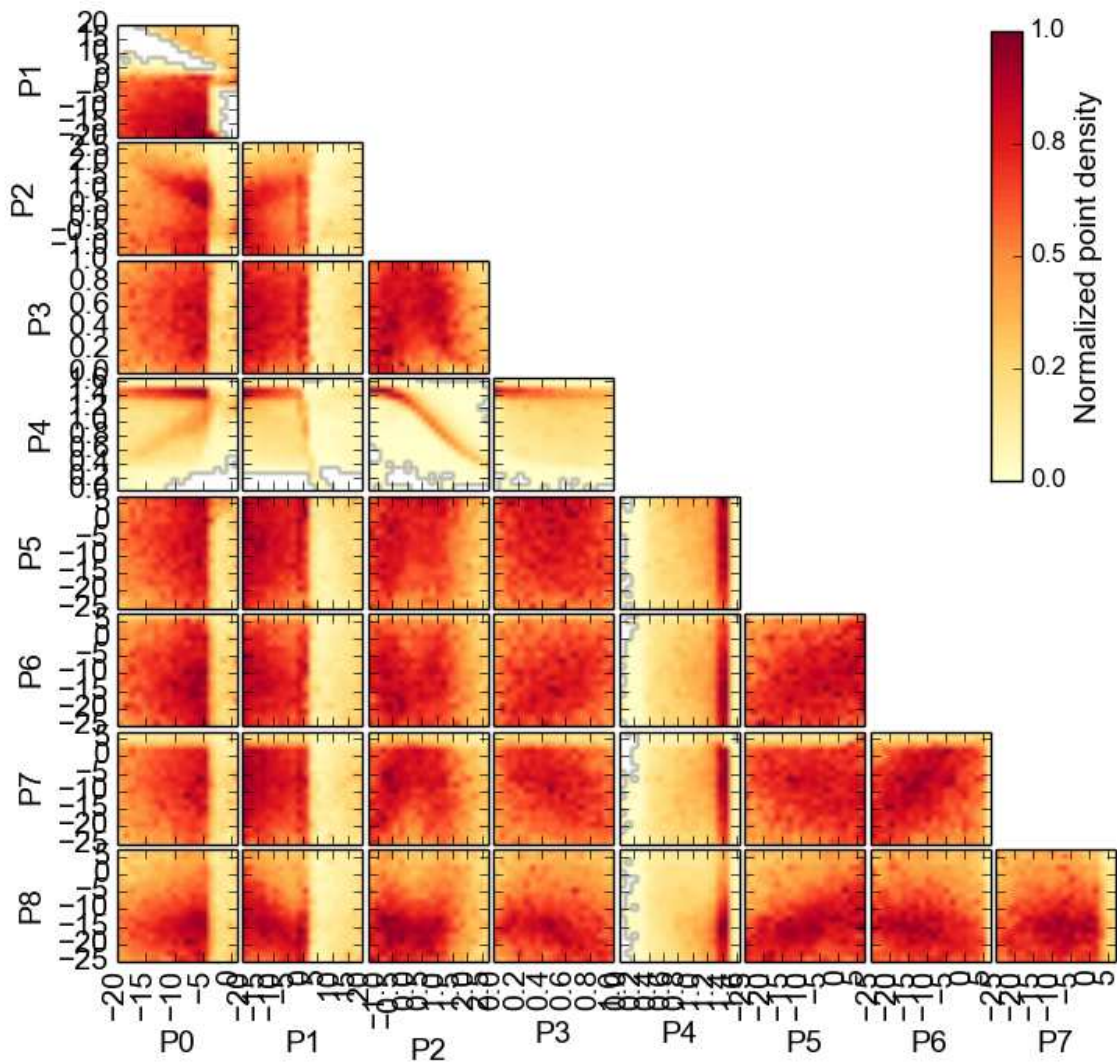
Figure 3.5:

These are the posterior distributions from Figure 3.4, plotted pairwise in two dimensional heatmaps with each other parameter. This is to help visualize plausible regions of the phase space.
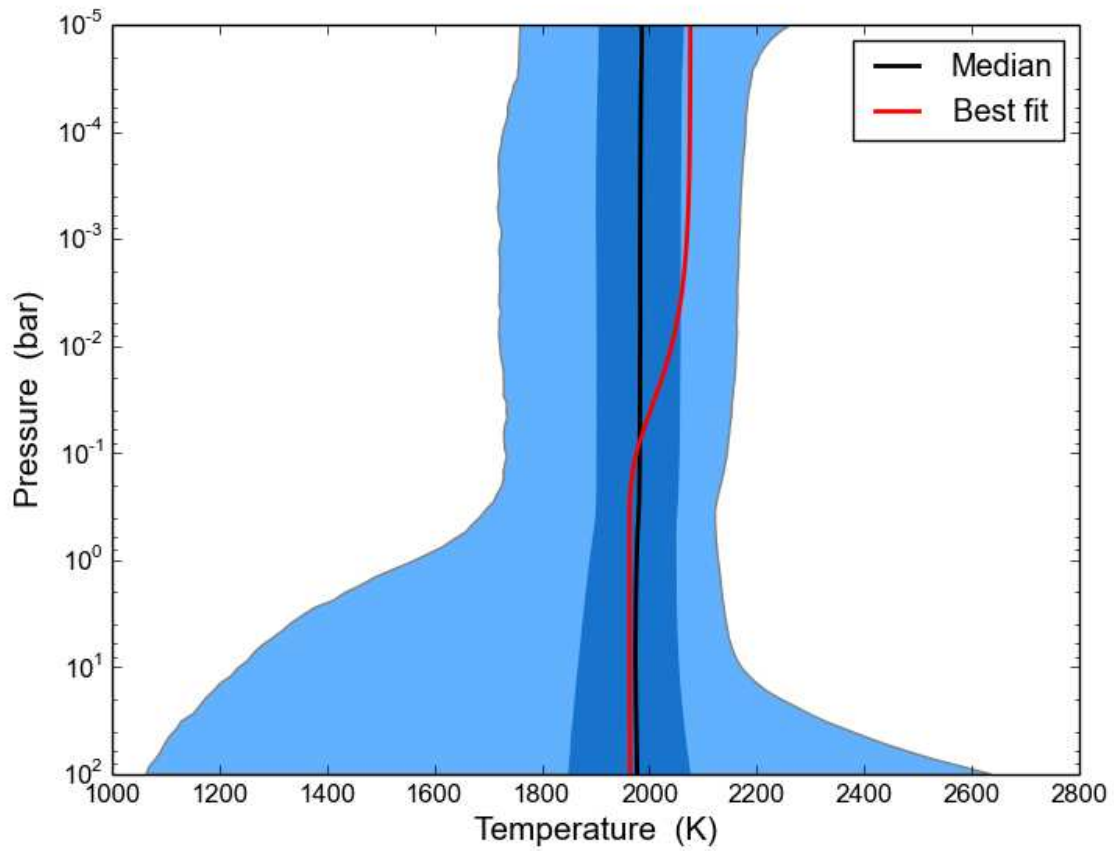
Figure 3.6:

This is the distribution of pressure-temperature profiles that were generated by the Markov chain. The dark blue region represents one sigma from the median (the black line), the light blue region represents all other generated PT profiles, and the red line represents the PT profile that gave the lowest χ^2.

CHAPTER 4: CONCLUSIONS

Spitzer took secondary eclipse observations of the exoplanet HAT-P-30-WASP-51Ab at 3.6 μm and 4.5 μm. They are well defined with signal-to-noise ratios of 9.6 and 10.4, respectively, but are possibly grazing eclipses. Although grazing eclipses can be useful for constraining the orbit of a planet, they present more complications for analyzing the planet's atmosphere because the eclipse depth is not representative of the entire dayside of the planet. This introduces an additional analysis complication that we did not attempt to address in this paper. We instead present a preliminary atmospheric model assuming that these are full eclipses, but they may not be. The brightness temperature of this planet from these eclipses is high enough to imply that most of the planet is eclipsed, and therefore these eclipse depths are approximately correct for a full eclipse.

With only two data points, we do not expect to constrain the composition of a planet, but we are able to constrain the temperature profile of this planet, particularly for upper atmosphere layers.

We were able to use the timing of our secondary-eclipse observations, together with transit-timing observations from the literature and amateur sources as well as radial-velocity data from both discovery papers and followup observations by the HATNet team to constrain the orbital parameters of this planet. We also present a constraint on $e\sin(\omega)$ using the assumption that this is a grazing eclipse. We find that a small but non-zero eccentricity is not unreasonable for this planet by comparing the age of the system to the circularization timescale of the planet.

This planet's large scale height should yeild high quality transit-spectroscopy, which will not be affected by the grazing secondary eclipse. The planet's low density raises the question of escape from the outer layers of its atmosphere.

LIST OF REFERENCES

Arras, P., Burkart, J., Quataert, E., & Weinberg, N. N. 2012, MNRAS, 422, 1761, provided by the SAO/NASA Astrophysics Data System

Bakos, G. Ã., Hartman, J. D., Penev, K., Csubry, Z., de Val-Borro, M., & Bhatti, W. A. 2015, HATNet Follow-up Data

Blecic, J. 2016, ArXiv e-prints, provided by the SAO/NASA Astrophysics Data System

Campo, C. J. et al. 2011, The Astrophysical Journal, 727, 125, provided by the SAO/NASA Astrophysics Data System

Charbonneau, D. et al. 2005, The Astrophysical Journal, 626, 523

Cubillos, P. et al. 2013, The Astrophysical Journal, 768, 42

Cubillos, P. E. 2016, ArXiv e-prints, provided by the SAO/NASA Astrophysics Data System

Deming, D., Brown, T. M., Charbonneau, D., Harrington, J., & Richardson, L. J. 2005, The Astrophysical Journal, 622, 1149

Deming, D. et al. 2015, The Astrophysical Journal, 805, 132

Enoch, B. et al. 2011, The Astronomical Journal, 142, 86

Goldreich, P., & Soter, S. 1966, Icarus, 5, 375

Johnson, J. A. et al. 2011, The Astrophysical Journal, 735, 24

Line, M. R. et al. 2013, The Astrophysical Journal, 775, 137

Mandel, K., & Agol, E. 2002, The Astrophysical Journall, 580, L171

Mardling, R. A. 2007, MNRAS, 382, 1768

Ngo, H. et al. 2015, The Astrophysical Journal, 800, 138

Nymeyer, S. et al. 2011, The Astrophysical Journal, 742, 35

Seager, S., & Deming, D. 2010, ARAA, 48, 631

Stevenson, K. et al. 2010, Nature, 464, 1161

Stevenson, K. B. et al. 2012a, The Astrophysical Journal, 754, 136

—. 2012b, The Astrophysical Journal, 755, 9

Wu, Y. 2005, The Astrophysical Journal, 635, 688